Journal of Nuclear Medicine, published on June 30, 2022 as doi:10.2967/jnumed.122.263838

First-in-human evaluation of ^{18}F-PF-06445974, a PET radioligand that preferentially labels phosphodiesterase-4B

Yuichi Wakabayashi[1], Per Stenkrona[2], Ryosuke Arakawa[2], Xuefeng Yan[1], Maia G. Van Buskirk[1], Madeline D. Jenkins[1], Jose A. Montero Santamaria[1], Kevin P. Maresca[3], Akihiro Takano[2], Jeih-San Liow[1], Thomas A. Chappie[3], Andrea Varrone[2], Sangram Nag[2], Lei Zhang[3], Zoë A Hughes[3], Christopher J. Schmidt[3], Shawn D. Doran[3], Andrew Mannes[4], Paolo Zanotti-Fregonara[1], Maarten Ooms[1], Cheryl L. Morse[1], Sami S. Zoghbi[1], Christer Halldin[2], Victor W. Pike[1], and Robert B. Innis[1]

[1]Molecular Imaging Branch, NIMH-NIH, Bethesda, MD, USA
[2]Department of Clinical Neuroscience Psychiatry Section, Karolinska Institutet, Stockholm, Sweden
[3]Worldwide Research, Development, and Medicine, Pfizer Inc, NY, USA
[4]Anesthesia Department, NIH Clinical Center, Bethesda, MD, USA

For submission to *Journal of Nuclear Medicine* as an Original Research Article, January 2022.
Revised March 2022.

Correspondence
Robert Innis, MD, PhD
Molecular Imaging Branch
NIMH-NIH
10 Center Drive, Rm. B1D43
Bethesda, MD 20892
Fax: +1-301-480-3610
Tel: +1-301-594-1368
Email: robert.innis@nih.gov

First Author
Yuichi Wakabayashi, MD, PhD
Postdoctoral Fellow, Molecular Imaging Branch
NIMH-NIH
10 Center Drive, Rm. B1D43
Bethesda, MD 20892
Fax: +1-301-480-3610
Tel: +1-301-594-1371

Financial Disclosures

This study was funded by the Intramural Research Program of the NIMH-NIH (ZIAMH002852 and ZIAMH002793) and by a research contract from Pfizer to the Karolinska Institutet.

Word Count: 4772

Running Title: Evaluation of ^{18}F-PF-06445974

ABSTRACT

Phosphodiesterase-4 (PDE4), which metabolizes the second messenger cyclic adenosine monophosphate (cAMP), has four isozymes: PDE4A, PDE4B, PDE4C, and PDE4D. PDE4B and PDE4D have the highest expression in brain and may play a role in the pathophysiology and treatment of depression and dementia. This study evaluated the properties of the newly developed PDE4B-selective radioligand ^{18}F-PF-06445974 in the brains of rodents, monkeys, and humans.

Methods: Three monkeys and five healthy human volunteers underwent positron emission tomography (PET) scans after intravenous injection of ^{18}F-PF-06445974. Brain uptake was quantified as total distribution volume (V_T) using the standard two-tissue compartment model and serial concentrations of parent radioligand in arterial plasma.

Results: ^{18}F-PF-06445974 readily distributed throughout monkey and human brain and had highest binding in the thalamus. The value of V_T was well identified by a two-tissue compartment model but increased by 10% during the terminal portions (40 and 60 minutes) of the monkey and human scans, respectively, consistent with radiometabolite accumulation in the brain. The average human V_T values for the whole brain were 9.5 ± 2.4 mL · cm^{-3}. Radiochromatographic analyses in knockout mice showed that two efflux transporters—permeability glycoprotein (P-gp) and breast cancer resistance protein (BCRP)—completely cleared the problematic radiometabolite but also partially cleared the parent radioligand from the brain. In vitro studies with the human transporters suggest that the parent radioligand was a partial substrate for BCRP and, to a lesser extent, for P-gp.

Conclusion: ^{18}F-PF-06445974 quantified PDE4B in human brain with reasonable, but not complete, success. The gold standard compartmental method of analyzing brain and plasma data successfully identified the regional densities of PDE4B, which were widespread and highest in the thalamus, as expected. Because the radiometabolite-induced error was only about 10%, the radioligand is, in the opinion of the authors, suitable to extend to clinical studies.

KEYWORDS: Phosphodiesterase-4B (PDE4B); PET; ^{18}F-PF-06445974

INTRODUCTION

Phosphodiesterase type 4 (PDE4) metabolizes and thereby inactivates the ubiquitous second messenger 3′,5′-cyclic adenosine monophosphate (cAMP). PDE4 inhibitors are approved to treat two peripheral inflammatory disorders (chronic obstructive pulmonary disease and psoriasis) and are being explored as treatments for several neuropsychiatric disorders *(1)*. PDE4 has four isozymes: PDE4A, PDE4B, PDE4C, and PDE4D; of these, the PDE4B and PDE4D isozymes are highly expressed in the brain and may play important roles in pathophysiology and treatment. Interestingly, inhibition of the PDE4D isozyme was found to improve cognition in animals and humans *(2)*, while inhibition of the PDE4B isozyme had antidepressant-like effects in animal models *(3)*. Subtype-selective inhibitors may not only be useful in treating distinct disorders but may also avoid the nausea and vomiting associated with non-selective inhibitors. For example, antidepressant trials of the non-selective PDE4 inhibitor rolipram were discontinued because of severe nausea and vomiting.

The search for subtype-selective PDE4 inhibitors has progressed in parallel with the development of comparable PET radioligands that can measure subtype density and evaluate whether the therapeutic candidate crosses the blood-brain barrier and engages the target—i.e., receptor occupancy. Subtype-selective PET radioligands have been developed for PDE4B (the subject of this paper) and PDE4D. However, the most promising PDE4D radioligand, ^{11}C-T1650, generated such a significant accumulation of radiometabolites in animal and human brain that it was not recommended for further study *(4)*. Such radiometabolites are problematic because quantitation of the target density is based on the assumption that all radioactivity in the brain is parent radioligand. If radiometabolites are included in brain signal, the density of the target will be overestimated.

^{18}F-PF-06445974, a new PET radioligand (Supplemental Figure S1), was developed to bind preferentially to PDE4B *(5)*. This ligand was selected as a candidate based on its in vitro properties and in vivo performance. In vitro, ^{18}F-PF-06445974 has high affinity (<1 nM) for PDE4B and moderate to high selectivity relative to the other three PDE4 subtypes (4.7 nM for PDE4A, 17 nM for PDE4C, and 36 nM for PDE4D). In vivo, PET imaging of ^{18}F-PF-06445974 in cynomolgus monkeys showed good brain

uptake, a high percentage of specific (i.e., blockable) binding, and robust quantitation of enzyme density using arterial input function of parent radioligand separated from radiometabolite *(5)*. Due to successful imaging in monkeys, the ligand was selected for first-in-human evaluation.

MATERIALS AND METHODS

This study sought to determine whether ^{18}F-PF-06445974 could accurately quantify PDE4B in living human brain. Towards this end, PET imaging was performed in healthy human volunteers using the gold standard method of compartmental modeling and serial concentrations of arterial plasma of parent radioligand separated from radiometabolite. Five volunteers were studied: three at the National Institutes of Health (NIH) and two at the Karolinska Institutet (KI). All participants gave written informed consent, and the study was approved by the IRBs of the respective institutions. To address the issue of potential radiometabolite accumulation in brain, in vivo studies in monkeys and in vivo and ex vivo studies in rodents were also performed following ^{18}F-PF-06445974 injection and blockade by non-radioactive PF-06445974. A detailed description of the methods and the relevant references (*6-11*) can be found in the Supplemental Materials.

RESULTS

Brain imaging

Uptake in the human brain was widespread (peak whole brain standardized uptake value (SUV) ~2-3) and highest in thalamus (Figures 1 and 2), consistent with the distribution of PDE4B (*12*). Plasma parent concentrations peaked immediately after injection and rapidly decreased along a curve that was well-fitted by a triexponential function (Fig. 2A). Brain activity achieved relatively stable peak values at 15-20 minutes and washed out slowly thereafter—i.e., only 17% washout from 20 to 120 minutes.

To quantify the density of the target enzyme in brain regions, pharmacokinetic modeling was performed using the serial concentrations of the parent radioligand in arterial plasma as the input to the brain—that is, it was assumed that the brain contains only parent radioligand and no radiometabolite. The

standard two-tissue compartment model provided curves that visually fit the measured PET values in a moderately good to excellent manner (Fig 2B). Total distribution volume (V_T) (mL · cm^{-3}) ranged from 6.4 in corpus callosum to 13.3 in thalamus (Table 1). The variability (SD) of the V_T measurements was quite large and due in part to differences between the two institutions. For example, for the V_T (mL·cm-) of whole brain in the five participants reported in Table 1, the NIH values were generally slightly lower (9.9, 9.9, 5.6) than those of the KI (10.2, 12.0). We do not know the cause(s) of these institutional differences but, in such a small population of participants, they could be due to chance. The V_T in human brain did not become stable during the 120-minute scan. Instead, V_T values increased by ~10% during the last 40 minutes of the scan (80-120 minutes; Figure 3A). This increase was similar in regions with high and low binding (Supplemental Figure S2).

Brain imaging in three monkeys (one rhesus monkey at the NIH and two cynomolgus monkeys at the KI) mirrored that in humans, including the indirect measure of radiometabolite accumulation. That is, V_T increased by ~10% during the last 60 minutes of the scan (120-180 minutes; Fig. 3B).

Assessing radiometabolite entry into brain

The number of radiometabolite peaks in plasma varied among rats, monkeys, and humans, but all radiometabolites were less lipophilic than the parent radioligand, as shown by eluting earlier in the reverse-phase high performance liquid chromatography (HPLC) (Supplemental Figure S3). Although less lipophilic, the major radiometabolite peak (marked with an asterisk in Supplemental Figure S3) eluted close enough to the parent radioligand that it would have been expected to enter the brain.

To directly determine whether this radiometabolite entered brain, three rats were euthanized 180 minutes post-radioligand injection, and radioactivity was extracted from brain and plasma. Virtually all (98±2%) radioactivity in brain co-eluted with the parent radioligand, whereas only 32% in plasma was parent radioligand (Figure 4). Thus, essentially none of the radiometabolite in rat plasma at 180 minutes was present in the brain.

To explain why rat brain had virtually no radiometabolite, brain uptake was measured in mice with a knockout of both permeability glycoprotein (P-gp) and breast cancer resistance protein (BCRP), the two most prevalent efflux transporters at the blood-brain barrier *(13).* Both the parent radioligand and the chromatographically adjacent radiometabolite were substrates for one or both efflux transporters in mice (Supplemental Figure S4). At 120 minutes post-^{18}F-PF-06445974 injection, the ratio of parent radioligand in brain to that in plasma was 93 in wild-type mice and 188 in knockout mice (Figure 5); because the concentrations in brain and plasma were in the same unit (SUV), the ratio is unitless. Thus, the brain to plasma ratio of parent radioligand was two times higher in knockout mice than in wild-type mice. Because these ratios of parent radioligand to brain to plasma were so high, this experiment was repeated in an additional set of three animals; similar results were obtained.

In these same mice at 180 minutes, the ratio of radiometabolite in brain to that in plasma was 0.2 in wild-type and 4.0 in knockout mice (i.e., a 20-fold difference), indicating that knockout of these two transporters had about a 10-fold greater effect (20 vs 2) on the radiometabolite than on the parent radioligand. This differential effect on the radiometabolite versus the parent radioligand was also seen in the percent composition of radioactivity in brain at 120 minutes. Specifically, the percentage of radiometabolite in brain was about five-fold higher in knockout (8.8%) than in wild-type (1.8%) mice (Supplemental Table S1).

Because substrate specificity varies between species, avidity was measured in vitro using cloned human transporters and compared to known substrates: digoxin for P-gp and prazosin for BCRP. For BCRP, prazosin had an efflux ratio of 9.2, whereas PF-06445974 had a ratio of 5.9 (Supplemental Table S2), suggesting that PF-06445974 was a mild/moderate substrate for BCRP. In contrast, PF-06445974 was a far less avid substrate for P-gp; specifically, digoxin had an efflux ratio of 38.1, and PF-06445974 had a ratio of only 2.5—i.e., less than 1/15th that for digoxin.

Like all metabolites, radiometabolites are often pharmacologically inactive by virtue of low affinity for the target protein. Thus, any displaceable binding typically reflects parent radioligand rather than radiometabolite. Nonradioactive PF-06445974 (0.1 mg/kg iv injected 10 minutes before the

radioligand) blocked almost all radioactivity in rat and monkey brain for the entire duration of the scan (Fig. 6, Supplemental Fig. S5). For the rhesus monkey, nonradioactive PF-06445974 decreased $SUV_{10\text{-}60}$ by 92% in the whole brain (Figure 6). In rats, nonradioactive PF-06445974 decreased $SUV_{10\text{-}180}$ by 94% in the whole brain (Supplemental Figure S5).

In summary, plasma from rats, monkeys, and humans showed a range of radiometabolites, all with lower—though sometimes only slightly lower—lipophilicities than that of ^{18}F-PF-06445974. None of these radiometabolites was present in rat brain 180 minutes after injection. Studies in knockout mice showed that the radiometabolite (the peaks marked with an asterisk in Supplemental Figures S3 and S4) adjacent to the radioligand was avidly cleared from the brain by P-gp and/or BCRP (Supplemental Figure S4). The monkey studies showed that 92% of brain radioactivity was blocked by non-radioactive ligand, suggesting that most of the radioactivity in monkey brain, like that in rats and mice, represented parent radioligand. Thus, by analogy to rats and monkeys, it is likely that no more than a small amount of radiometabolite (≤ 10% of total radioactivity) accumulates in human brain. However, of particular importance to the quantitation of enzyme density, the in vitro studies showed that the parent radioligand is a moderate substrate for human BCRP.

Dosimetry calculations in human and nonhuman primates

Whole-body imaging in two humans and one monkey was notable for early distribution in the blood pool, accumulation in the target organs (i.e., brain and lung), and excretion via urinary tract (Supplemental Fig. S6). For the human volunteers, the four organs with the highest exposure (μSv/MBq) were gallbladder (110±75), upper large intestine (75±66), urinary bladder (55±5.9), and liver (44±8.1). The doses in the two humans were 19.6 and 19.3 μSv/MBq, respectively, which were similar to those extrapolated from monkeys (16.5 μSv/MBq) (Supplemental Table S3).

DISCUSSION

This study sought to determine whether ^{18}F-PF-06445974 could accurately quantify PDE4B in human brain. Our results suggest that this radioligand quantified PDE4B reasonably well, with the exception that radiometabolite likely accumulated in brain and that the radioligand itself may be a substrate for efflux transport from the brain. Brain uptake was moderately high (peak whole-brain SUV was 1.5), and its distribution was appropriate for the target. The PET measurements of enzyme binding (V_T) from human brain were reasonably well fit to a two-tissue compartment model that assumed input of only the parent radioligand from arterial plasma. The V_T value increased by ~10% over the last 60 minutes of the 120-minute scan (Figure 3), which may have been caused by radiometabolite accumulation in the brain.

To directly measure radiometabolite, all radioactivity was extracted from plasma and brain of rats at 180 minutes and the components were separated using radio-HPLC. Surprisingly, rat brain contained essentially no radiometabolite, although the plasma had several radiometabolites, one of which eluted only slightly before the parent radioligand. Knockout of two efflux transporters (P-gp and BCRP) in mice showed that the radiometabolite was avidly cleared from the brain and that the parent radioligand was also a substrate, but of lower avidity. Thus, either or both efflux transporters had the positive effect of "cleaning up" the brain signal by removing radiometabolite, but also the negative effect of removing some of the parent radioligand. In vitro studies using cloned human efflux transporters showed that PF-06445974 was a moderate substrate for BCRP and, to a lesser extent, for P-gp. Although these efflux transporters completely cleared radiometabolite from rodent brain, they likely did so only partially in humans, leading to the accumulation of the adjacent radiometabolite in human brain, as shown by increasing values of enzyme density with increasing length of scanning.

Compartmental modeling seeks to measure the specific binding (V_S) of the radioligand for the target and is proportional to receptor density (B_{max}) times the radioligand's affinity ($1/K_D$). Because the measurements of PET radioactivity in brain and of parent radioligand in plasma have noise, a 'substantial' number of such measurements are required to converge on a value of specific binding, often 15-60

minutes for many brain radioligands. If the density of the target and the affinity of the radioligand remain constant during the scan, the converged/well-identified V_S value should not change with increasing scan duration, which will be reflected by the brain and plasma time-activity curves decreasing at the same rate. In contrast, in this study, values of total uptake (V_T=V_S+V_{ND}) appeared to increase with increasing scan duration.

The two most common causes of unstable V_T values are slow kinetics of radioligand binding and/or the accumulation of radiometabolites in the brain. The first possible cause, slow kinetics, refers to how long the radioligand requires to reach "equilibrium," which in this case usually refers to the time of peak radioactivity in brain; note that the term "peak equilibrium" refers to tissue to plasma ratio at the exact time of peak uptake in the brain, which varies among regions. This peak equilibrium is distinct from "transient equilibrium" (*14*), which refers to the tissue to plasma ratio after the time of peak uptake and which is typically greater than the true V_T. As a rule, the brain must be imaged before, at, and for some time after peak uptake to quantify the rates of binding and unbinding to the receptor, which themselves are components of V_T. Here, the time to peak was about 30 minutes in monkeys and 20 minutes in humans, and our scans extended well beyond the peak (for a total of 180 minutes in monkeys and 120 minutes in humans), suggesting that slow kinetics of radioligand binding are unlikely to have caused the V_T values that increased with scan duration. Instead, radiometabolite probably accumulated in the human brain. The likely candidate is the peak marked with an asterisk in Supplemental Figure S3, which has lipophilicity only slightly lower than that of the parent radioligand.

It should be noted that being a substrate for efflux transport is unlikely to increase V_T values over time, as it is predicted to have the opposite result. That is, the effect of efflux transport is to decrease radioactivity in brain and, therefore, to decrease the V_T. Nevertheless, the time course of efflux transport of parent ligand and radiometabolite might change in some unexpected way to contribute to increasing values of V_T.

Taken together, the results suggests that the two pharmacological limitations of ^{18}F-PF-06445974 for quantifying PDE4B in human brain are the accumulation of a radiometabolite in the brain and partial

removal of the parent radioligand by the efflux transporter BCRP. Both pharmacological limitations will increase the variability of the measurements between individuals to the extent that individuals differ in metabolism and BCRP function. The severity of these combined limitations in humans is unknown but, in the opinion of the authors, would not preclude using this radioligand in clinical studies. An increase in V_T of <5% during the last hour is considered excellent, and our rate of 10% in the last 60 minutes (Figure 3) is generally considered acceptable. Notably, this 10% variability mirrors what might maximally occur based on blockade studies in monkeys (Figure 6). That is, nonradioactive PF-06445974 blocked 92% of total uptake in monkey brain, suggesting that 92% of radioactivity in brain was parent radioligand; metabolites usually, but not always, have lower affinity for the target than the parent drug.

Although these two limitations will increase the necessary sample size for a clinical study, we will proceed with use of this radioligand to study clinical disorders such as major depressive disorder (MDD) for two reasons. First, as described above, the error/variability of these limitation may only be about 10%. Second, PET imaging of PDE4 provides the unique ability to measure the activated (i.e., phosphorylated) form of PDE4, which is not possible in postmortem samples (Figure 7). Prior studies in this laboratory with ^{11}C-(*R*)-rolipram, which binds to all four PDE4 subtypes, provide in vivo support for the notion that cAMP increases radioligand binding via phosphorylation of PDE4 by protein kinase A (PKA) *(15)*. This phosphorylation increases enzyme activity as well as the affinity of radioligand binding by about 10-fold *(16)*. Because PDE4 is rapidly dephosphorylated after death *(17)*, PET is uniquely capable of measuring the active form of PDE4 in living participants.

Evidence from the 1980s and 1990s suggested that rolipram might be used to treat MDD, and animal models of depression suggested that PDE4B inhibitors might have antidepressant efficacy in humans *(3)*. In this context, a PET radioligand for PDE4B could facilitate therapeutic drug development. For instance, we predict that the current study using a PDE4B selective radioligand will replicate results previously obtained with the non-selective radioligand ^{11}C-(*R*)-rolipram *(18)*—namely, that PDE4B binding will be decreased in unmedicated individuals experiencing a major depressive episode but still have significant overlap with that in healthy volunteers. If so, this PDE4B radioligand could be used to

identify a subgroup of MDD patients who would most benefit from PDE4B inhibition, given that low PDE4 binding implies low cAMP signaling because of the negative feedback mechanism mediated by PKA. The cAMP theory of the mechanism of antidepressant treatments would further suggest that increasing cAMP signaling produces antidepressant effects. Thus, those patients with low PDE4B binding might be most likely to benefit from treatment with a PDE4B inhibitor. Furthermore, numerous animal studies have shown that antidepressants of all chemical classes must be administered for several weeks in order to upregulate the cAMP cascade *(19)*, which mirrors the therapeutic time-course in humans. Because inhibiting PDE4B would immediately increase cAMP signaling, these antidepressant effects, if they exist, would occur quickly, meaning that PDE4B inhibitors may represent a new class of rapid-acting antidepressants.

In short, a PET radioligand for PDE4B may be useful in two ways. First, if a PDE4B inhibitor is developed as an antidepressant medication, the PET radioligand can be used to identify the appropriate dose and dosing interval of the therapeutic candidate. Indeed, PET radioligands have often been used to measure "receptor occupancy" and guide initial doses in therapeutic trials. Second, a PDE4B radioligand might identify a subgroup of patients most likely to respond to a PDE4B inhibitor. This selection of patients likely to respond has been referred to as patient stratification, patient enrichment, personalized medicine and, most recently, precision medicine. Expressed in other terms, low PDE4B binding may be a biomarker to predict response to a PDE4B inhibitor.

CONCLUSION

^{18}F-PF-06445974 was able to quantify PDE4B in human brain with reasonable, but not complete, success. The gold standard compartmental method of analyzing brain and plasma data successfully identified the regional densities of PDE4B, which were widespread and highest in the thalamus, as expected. Although a radiometabolite may contaminate the signal in human brain, the amount is likely small enough (~10%) that the authors plan to use this radioligand in clinical studies.

FINANCIAL DISCLOSURE

This study was funded by the Intramural Research Program of the National Institute of Mental Health (projects ZIAMH002852 and ZIAMH002793; animal protocol: MIB-02) and by a research contract from Pfizer to the Karolinska Institutet.

DISCLAIMER

The following authors have no conflicts of interest to disclose, financial or otherwise: Wakabayashi, Yan, Van Buskirk, Jenkins, Montero Santamaria, Liow, Mannes, Zanotti-Fregonara, Ooms, Morse, Zoghbi, Pike, and Innis. The following Karolinska Institutet authors were supported by a contract with Pfizer: Stenkrona, Arakawa, Takano, Varrone, Nag, and Halldin. The following authors were full-time employees of Pfizer: Maresca, Chappie, Zhang, Hughes, Schmidt, and Doran.

ACKNOWLEDGEMENTS

The authors are grateful to the staff of Molecular Imaging Branch for participant recruitment; to the NIH's PET Department (Chief, Peter Herscovitch, MD) for performing the PET scans; to Ioline Henter for invaluable editorial assistance; and to Cerevel Therapeutics for obtaining the in vitro potencies of PF-06445974 at human P-gp and BCRP transporters.

KEY POINTS

Question: This study sought to determine whether ^{18}F-PF-06445974 can accurately quantify PDE4B in living human brain.

Pertinent Findings: ^{18}F-PF-06445974 can accurately quantify PDE4B, except for the likely presence of a small amount (probably ~10%) of radiometabolite in brain and the removal of the radioligand from the brain via an efflux transporter.

Implications for Patient Care: These findings have no direct implications for clinical care. However, a radioligand selective for PDE4B could measure this target in clinical disorders and facilitate the development of PDE4B-selective inhibitors as novel therapeutics.

REFERENCES

1. Menniti FS, Faraci WS, Schmidt CJ. Phosphodiesterases in the CNS: targets for drug development. *Nat Rev Drug Discov.* 2006;5:660-670.

2. Berry-Kravis EM, Harnett MD, Reines SA, et al. Inhibition of phosphodiesterase-4D in adults with fragile X syndrome: a randomized, placebo-controlled, phase 2 clinical trial. *Nat Med.* 2021;27:862-870.

3. Zhang C, Xu Y, Zhang H-T, Gurney ME, O'Donnell JM. Comparison of the pharmacological profiles of selective PDE4B and PDE4D inhibitors in the central nervous system. *Sci Rep.* 2017;7:40115.

4. Wakabayashi Y, Telu S, Dick RM, et al. Discovery, radiolabeling, and evaluation of subtype-selective inhibitors for positron emission tomography imaging of brain phosphodiesterase-4D. *ACS Chem Neurosci.* 2020;11:1311-1323.

5. Zhang L, Chen L, Beck EM, et al. The discovery of a novel phosphodiesterase (PDE) 4B-preferring radioligand for positron emission tomography (PET) imaging. *J Med Chem.* 2017;60:8538-8551.

6. Hammers A, Allom R, Koepp MJ, et al. Three-dimensional maximum probability atlas of the human brain, with particular reference to the temporal lobe. *Hum Brain Mapp.* 2003;19:224-247.

7. Innis RB, Cunningham VJ, Delforge J, al e. Consensus nomenclature for in vivo imaging of reversibly binding radioligands. *J Cereb Blood Flow Metab.* 2007;27:1533-1539.

8. National Research Council. *Guide for the Care and Use of Laboratory Animals, Eighth Ed.* Washington, DC: National Academies Press; 2011.

9. Sprague DR, Fujita M, Ryu YH, Liow JS, Pike VW, Innis RB. Whole-body biodistribution and radiation dosimetry in monkeys and humans of the phosphodiesterase 4 radioligand [(11)C](R)-rolipram: comparison of two-dimensional planar, bisected and quadrisected image analyses. *Nucl Med Biol.* 2008;35:493-500.

10. Terry G, Liow JS, Chernet E, et al. Positron emission tomography imaging using an inverse agonist radioligand to assess cannabinoid CB1 receptors in rodents. *Neuroimage.* 2008;41:690-698.

11. Zoghbi SS, Shetty HU, Ichise M, et al. PET imaging of the dopamine transporter with ^{18}F-FECNT: a polar radiometabolite confounds brain radioligand measurements. *J Nucl Med.* 2006;47:520-527.

12. Richter W, Menniti FS, Zhang H-T, Conti M. PDE4 as a target for cognition enhancement. *Expert Opin Ther Targets*. 2013;17:1011-1027.

13. Löscher W, Potschka H. Blood-brain barrier active efflux transporters: ATP-binding cassette gene family. *NeuroRx.* 2005;2:86-98.

14. Carson RE. PET physiological measurements using constant infusion. *Nucl Med Biol.* 2000;27:657-660.

15. Itoh T, Abe K, Hong J, et al. Effects of cAMP dependent protein kinase activator and inhibitor on in vivo PET rolipram binding to phosphodiesterase 4 in conscious rats. *Synapse.* 2010;64:172-176.

16. Hoffman R, Wilkinson IR, McCallum JF, Engels P, Houslay MD. cAMP-specific phosphodiesterase HSPDE4D3 mutants which mimic activation and changes in rolipram inhibition triggered by protein kinase A phosphorylation of Ser-54: generation of a molecular model. *Biochem J.* 1998;333:139-149.

17. Itoh T, Abe K, Zoghbi SS, et al. PET measurement of the in vivo affinity of 11C-(R)-rolipram and the density of its target, phosphodiesterase-4, in brain of conscious and anesthetized rats. *J Nucl Med.* 2009;50:749-756.

18. Fujita M, Richards EM, Niciu MJ, et al. cAMP signaling in brain is decreased in unmedicated depressed patients and increased by treatment with a selective serotonin reuptake inhibitor. *Mol Psychiatry.* 2017;22:754-759.

19. Duman RS. Synaptic plasticity and mood disorders. *Mol Psychiatry.* 2002;7 Suppl 1:S29-S34.

FIGURE LEGENDS

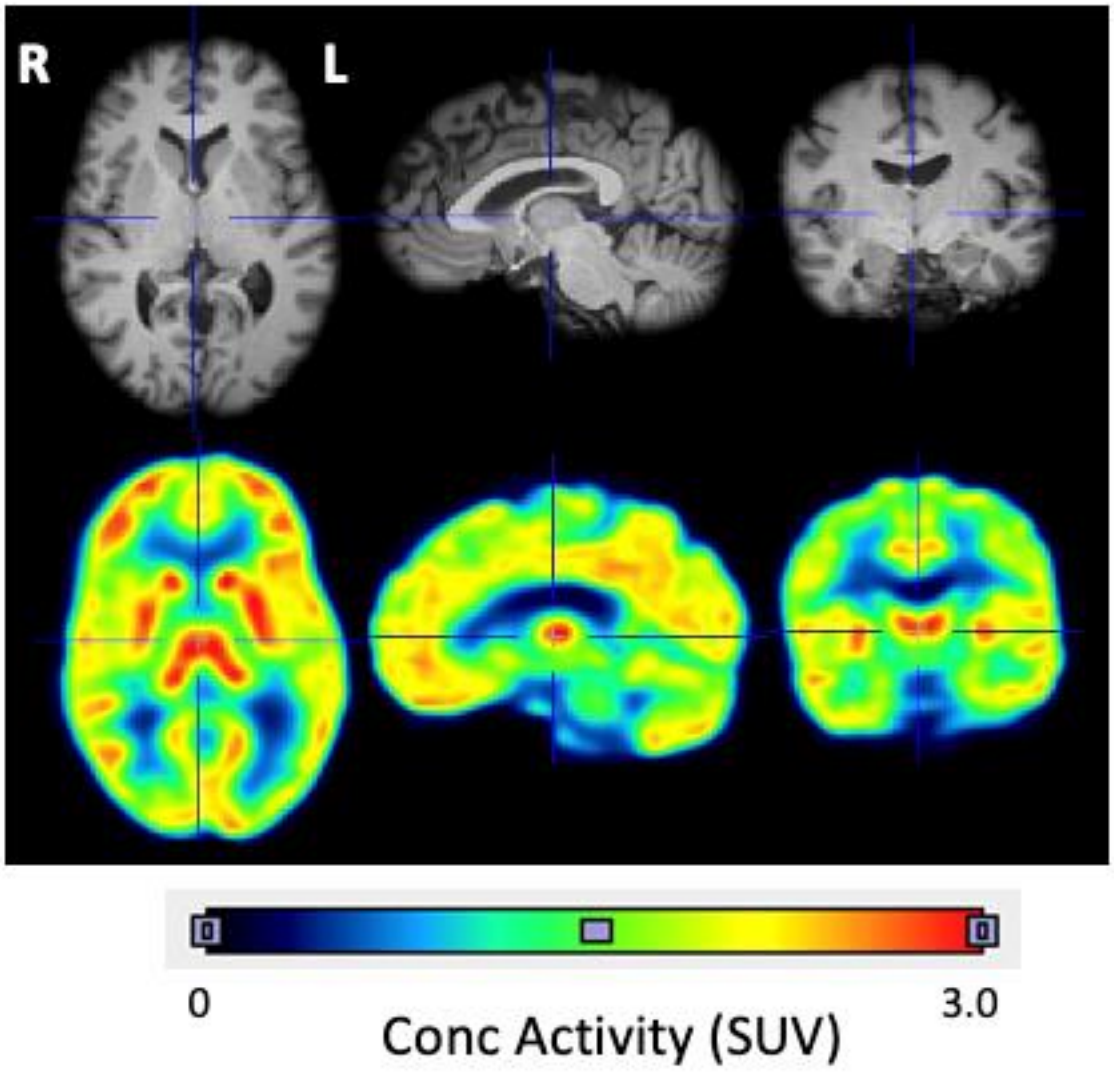

FIGURE 1. Distribution of radioactivity in the brain of a healthy volunteer after injection of ^{18}F-PF-06445974 and the participant's co-registered magnetic resonance imaging (MRI) scan. The positron emission tomography (PET) image displays the mean concentration of radioactivity from 0 to 120 minutes and is expressed as standardized uptake value (SUV). The highest uptake was in the thalamus, which is marked with cross hairs.

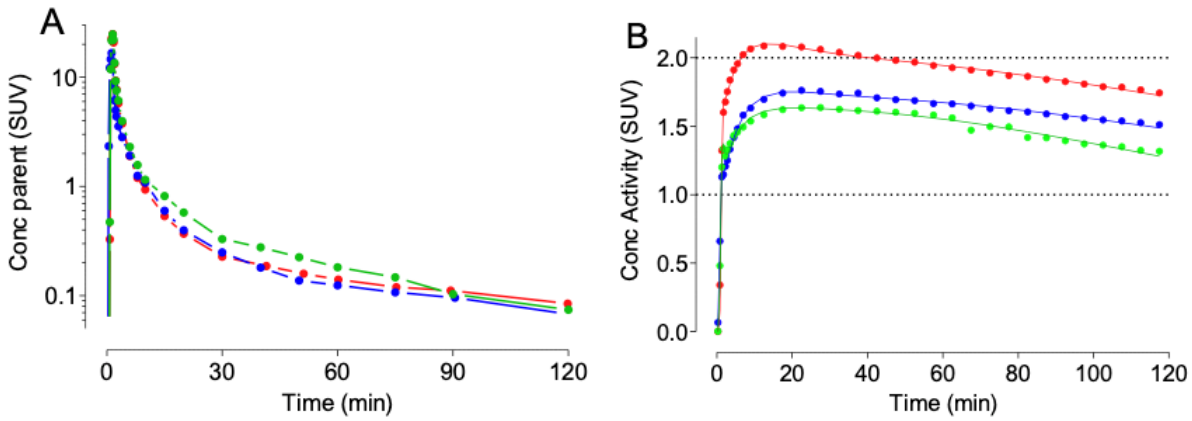

FIGURE 2. Concentration of (A) plasma parent radioligand ^{18}F-PF-0644974 separated from radiometabolite and (B) total radioactivity in the whole brain of three healthy human participants. The plasma time-activity curve after the peak was fit to a triexponential curve. The brain time-activity curve was fit to a two-tissue compartment model. The concentrations in plasma and brain are expressed as standardized uptake value (SUV). Note that the plasma parent is plotted on a log scale, and the brain activity is plotted on a linear scale.

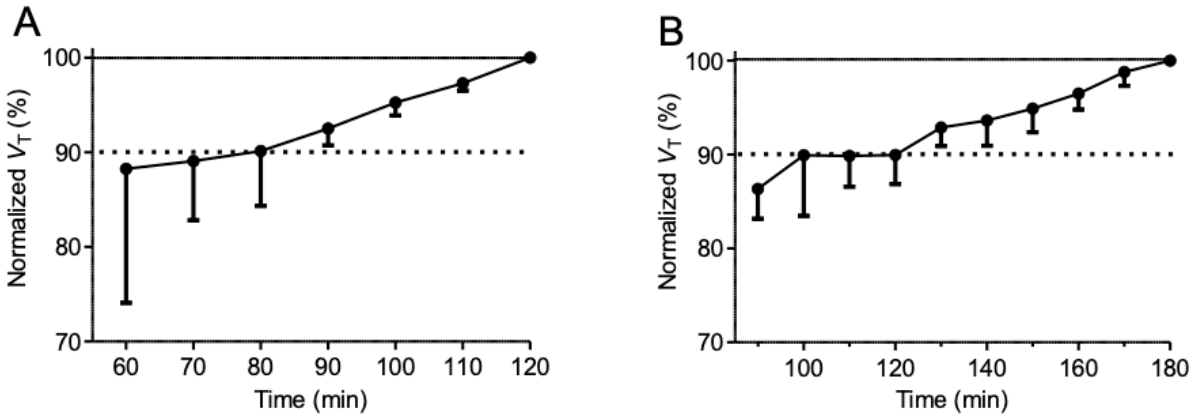

FIGURE 3. The value of total distribution volume (V_T) from (A) five human participants and (B) three monkeys. V_T values never achieved stability during the scans. V_T values increased linearly by 10% during the last 40 minutes in humans and also by 10% during the last 60 minutes in monkeys.

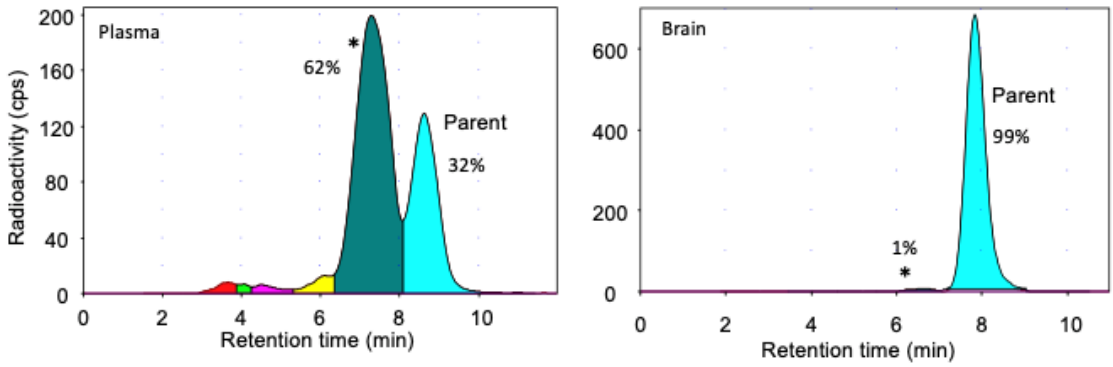

FIGURE 4. Radiochromatograms showing the composition of radioactivity extracted at 180 minutes from (A) plasma and (B) brain of a rat injected with ^{18}F-PF-06445974. In plasma (A), the parent radioligand (blue peak) composed 32% of total radioactivity, and the adjacent radiometabolite (peak marked with an asterisk) was 62%. At the same time, in the brain (B), the parent radioligand composed 99% of total radioactivity while the adjacent radiometabolite was only 1%.

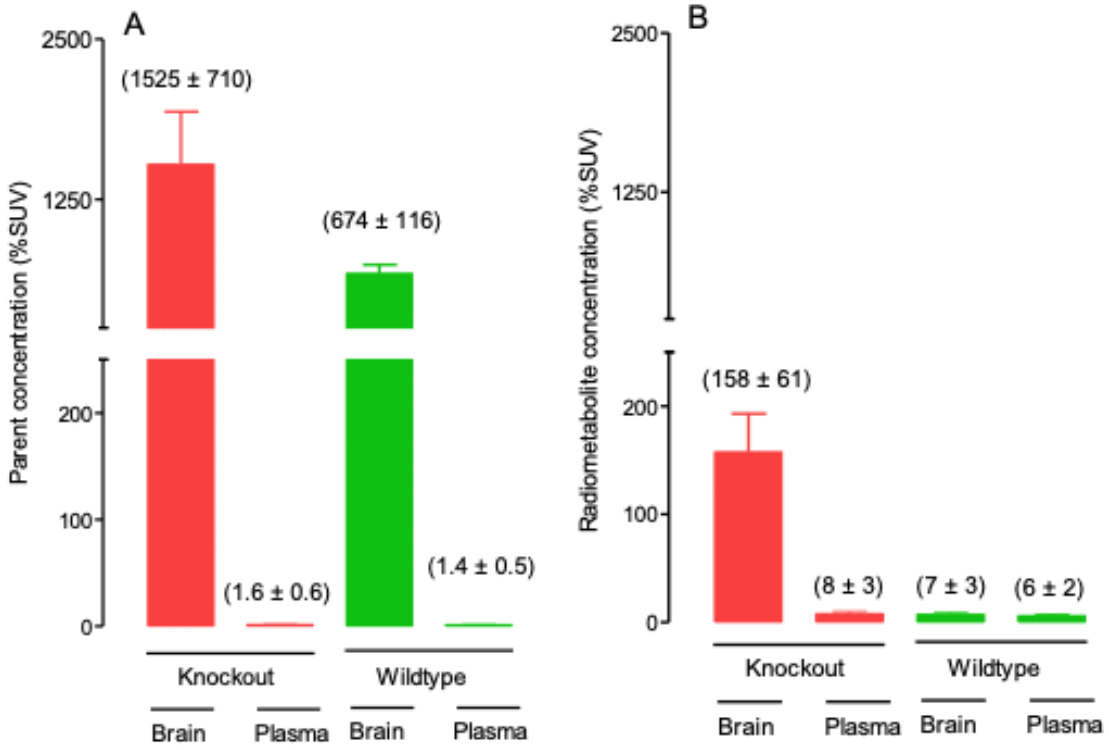

FIGURE 5. Concentrations of parent radioligand in brain and plasma of wild-type and efflux transporter knockout mice at 120 minutes after ^{18}F-PF-06445974 injection. (A) For the parent radioligand, the ratio of brain to plasma concentration was 93 in wild-type and 188 in mice with a knockout of both breast cancer resistance protein (BCRP) and permeability glycoprotein (P-gp). Thus, the brain to plasma ratio of parent radioligand was two times higher in knockout mice than in wild-type mice. (B) For the radiometabolite, the ratio of brain to plasma concentration was 0.2 in wild-type and 14.0 in BCRP and P-gp knockout mice. Thus, the brain to plasma ratio of parent radioligand was 20 times higher in knockout mice than in wild-type mice. Concentrations are expressed as percent standardized uptake value (%SUV).

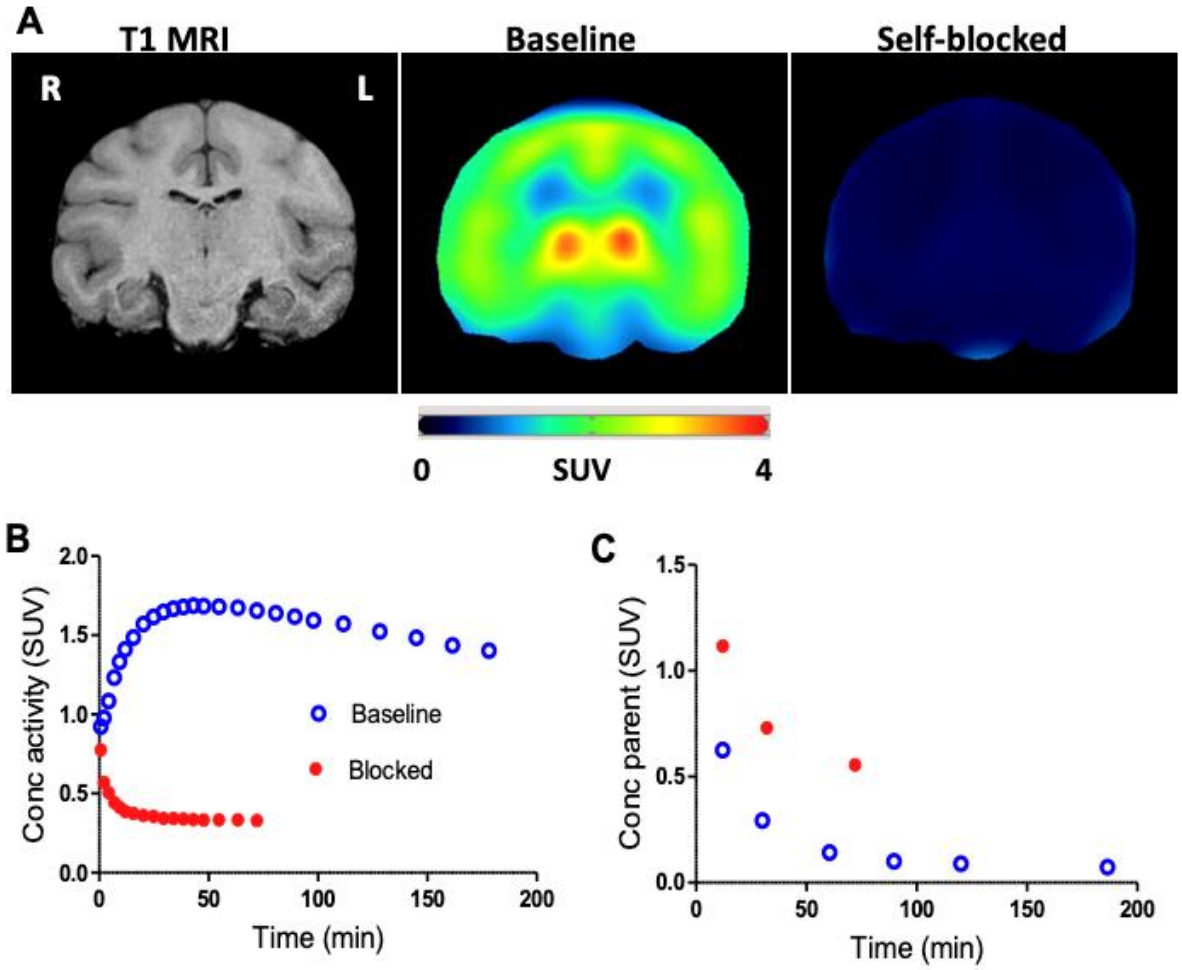

FIGURE 6. (A) Positron emission tomography (PET) and co-registered magnetic resonance imaging (MRI) of brain in a rhesus monkey. The animal was scanned at baseline and after blockade by PF-06445974 (0.1 mg/kg i.v. injected 10 minutes prior to the radioligand). Due to prolonged tachycardia (heart rate up to 190 bpm), the blocked scan was terminated after 75 minutes. The PET images show the mean concentration of radioactivity standardized uptake value (SUV) from 0 to 70 minutes. (B) Radioactivity in the whole brain after injection of ^{18}F-PF-06445974. (C) Concentration in arterial plasma of plasma parent radioligand ^{18}F-PF-06445974 separated from radiometabolite. Because there were so few plasma samples, compartmental modeling could not generate a reliable measure of enzyme density (total distribution volume, V_T). Measured as the average concentration of radioactivity from 10 to 60 minutes ($SUV_{10\text{-}60}$), non-radioactive PF-06445974 blocked 92% of radioligand uptake into brain.

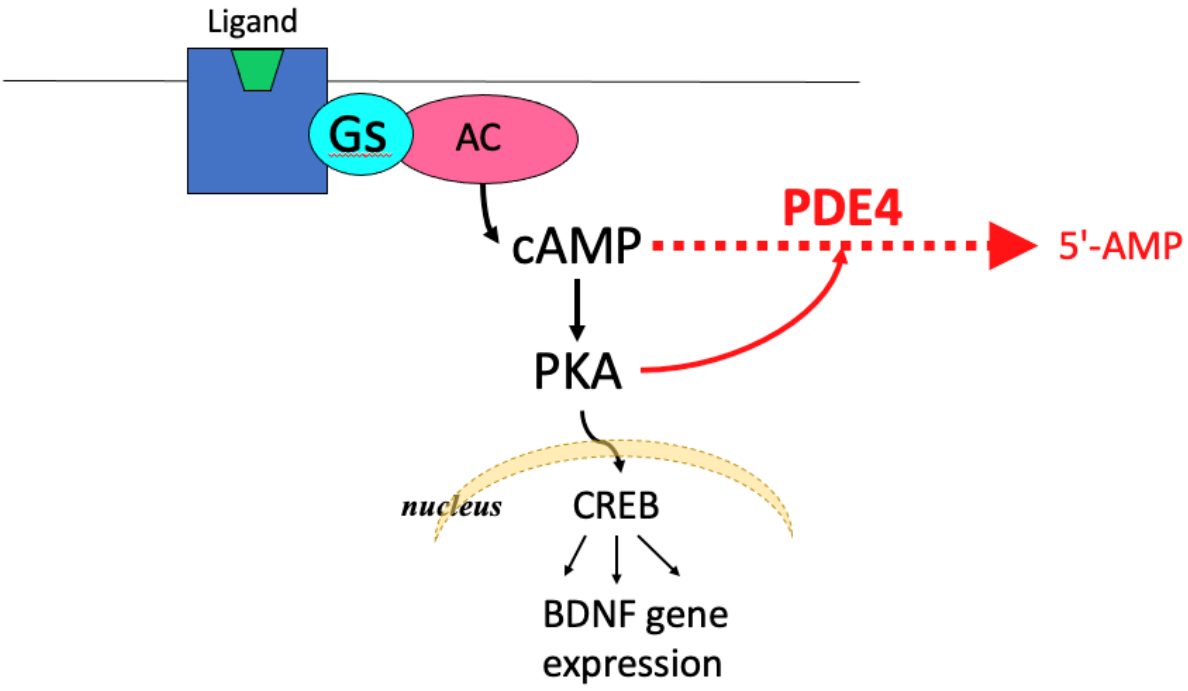

FIGURE 7. Schema of the cyclic adenosine monophosphate (cAMP) cascade (black arrows) and negative feedback via protein kinase A (PKA) (red arrows). Several neurotransmitters act via receptors coupled to G proteins (Gs) to stimulate adenylate cyclase (AC), which produces cAMP, activates PKA, and then phosphorylates cAMP response element-binding protein (CREB), which moves to the nucleus and increases expression of brain-derived neurotrophic factor (BDNF) and other genes. Negative feedback is provided by PKA, which phosphorylates and activates phosphodiesterase-4 (PDE4), which metabolizes cAMP, thereby terminating the cAMP signal.

TABLE 1. Total distribution volume (V_T) in brain regions for five human participants.

	V_T (mL · cm^{-3})	
Region	Mean	SD
Whole brain	9.5	2.4
Frontal cortex	9.5	2.6
Cingulate	9.8	3.2
Hippocampus	9	2
Amygdala	11.2	2.5
Temporal cortex	9.8	2
Parietal cortex	9.3	2.7
Occipital cortex	8.9	2.2
Striatum	12.1	2.7
Thalamus	13.3	3.4
Globus pallidus	12.2	5.6
Corpus callosum	6.4	3.8
Insula	10.8	2.7
Cerebellum	10.6	2.2

Graphical Abstract

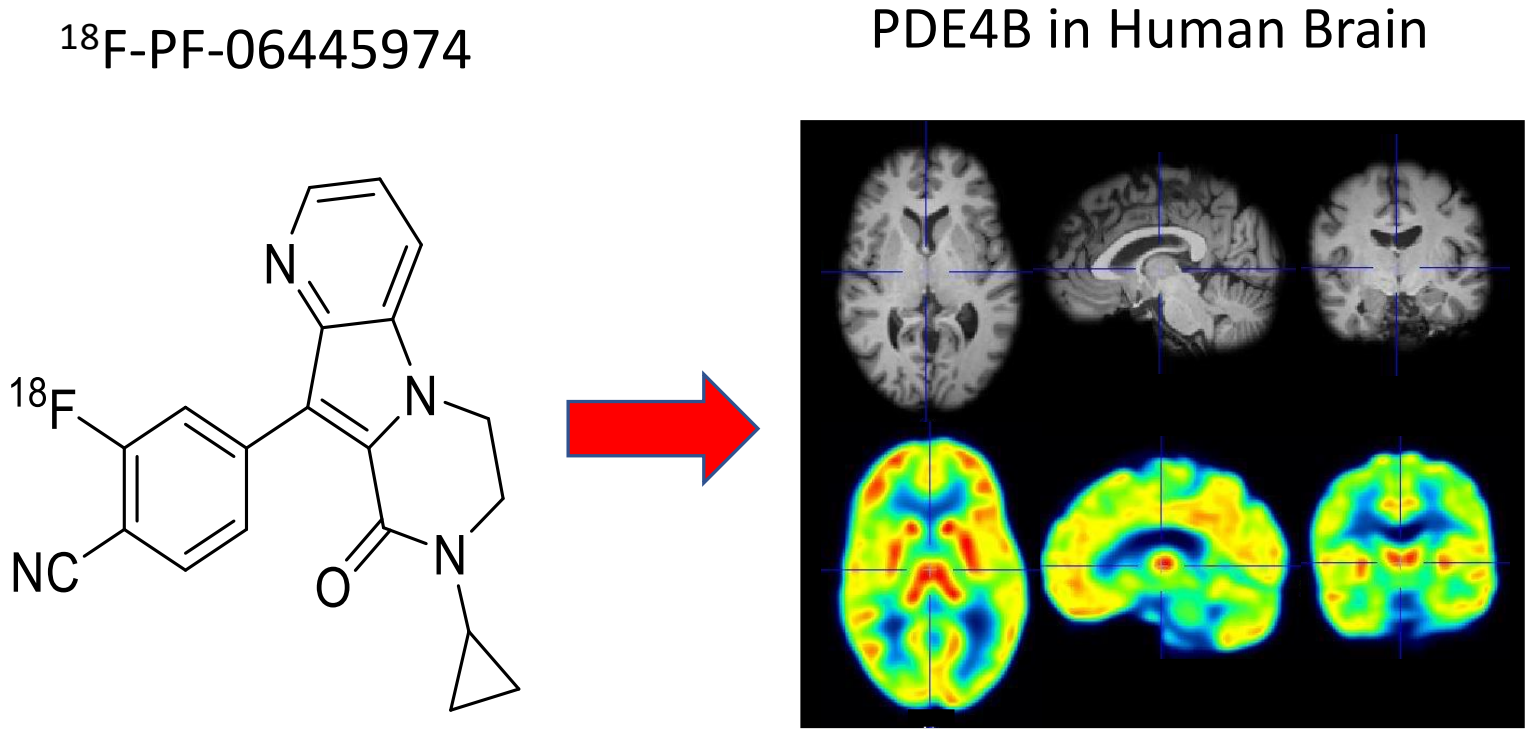

SUPPLEMENT

Supplemental Methods

Radioligand synthesis

^{18}F-PF-06445974 was synthesized using a nucleophilic substitution of ^{18}F-fluoride on a nitro-aryl precursor, as previously described *(1)*. The mean and standard deviation of the administered mass of ^{18}F-PF-06445974 was 1.0 ± 0.8 μg (range: 0.2–2.5), the mean administered activity was 180 ± 48 MBq (range: 77–226), and the mean molar activity was 93 ± 51 GBq/μmol (range: 31-163). No adverse or clinically detectable pharmacologic effects were noted in any of the seven participants (five for brain imaging and two for whole-body imaging). No significant changes were observed in vital signs or in the results of laboratory studies or electrocardiograms.

PET scanning in human brain

Five healthy volunteers (three male and two female; average age: 32.2±13.2 years; average body weight: 78.2±16.6 kg) were scanned with ^{18}F-PF-06445974. All participants gave written informed consent, and the study was approved by the IRBs of the respective institutions.

At the NIH, scans were performed with a Biograph mCT (Siemens Healthineers; Erlangen, Germany). CT scans for attenuation correction were acquired before radioligand injection. Following a one-minute intravenous bolus injection of 194±4.4 MBq of ^{18}F-PF-06445974, brain dynamic emission scans were obtained for 120 minutes. PET images were reconstructed with order subset expectation maximization (OSEM). At the KI, scans were performed with the ECAT EXACT HR (Siemens Healthineers) system. A transmission scan with three rotating ^{68}Ge sources was acquired for attenuation correction for approximately 10 minutes. After bolus injection of 202±19.6 MBq of ^{18}F PF-06445974, emission scans were acquired for 120 minutes. PET images were reconstructed with correction for attenuation and scatter using filtered-back projection.

A radiometabolite-corrected input function was obtained from arterial samples. At the NIH, the concentration of parent radioligand in the plasma and whole blood was measured manually every 15 seconds until three minutes and then at 4, 6, 8, 10, 15, 30, 40, 50, 60, 75, 90, and 120 minutes. At the KI, arterial blood was collected continuously for five minutes using an automated blood sampling system at a speed of 5 mL/min. Manual samples were also collected every minute during the first 5 minutes and then at 6, 8, 10, 20, 30, 45, 60, 90, and 120 minutes.

Because the acquisition times differed between the NIH and the KI, data from the first 120 minutes, which were available for all participants, were analyzed. Eighty-three predefined regions of interest (ROIs) from the Hammers N30R83 Maximum Probability Atlas *(2)* derived from the individual's MRI scan were applied to the co-registered dynamic PET images to obtain regional time-activity curves. For better representation and noise reduction, the 83 ROIs were subsequently combined via weighted averaging into 13 regions (frontal cortex, cingulate, hippocampus, amygdala, temporal cortex, parietal cortex, occipital cortex, striatum, thalamus, globus pallidus, corpus callosum, insula, and cerebellum). Total distribution volume (V_T) for each region was calculated using two-tissue compartment modeling *(3)*. The stability of V_T values over time was evaluated by incrementally decreasing the period of brain data from 120 to 60 minutes and calculating the relative V_T of the truncated scan to V_T of the full scan. All PET images were analyzed using PMOD 3.9 (PMOD Technologies Ltd., Zurich, Switzerland).

Whole-body scanning and dosimetry estimates in human and monkey

To estimate radiation exposure in humans, whole-body scanning was first performed in monkeys after correction for the species-dependent ratios of organ to body mass *(4)*. To determine the radiation exposure to body organs directly in humans, two 26 year-old healthy volunteers (one male and one

female) underwent a whole-body PET scan after intravenous injection of ^{18}F-PF-06445974 (77.0 and 52.0 MBq, respectively). Dynamic whole-body scans were acquired in seven contiguous segments from the top of the head to mid-thigh with 14 frames of increasing duration (75 seconds to 15 minutes) and a total scan time of 120 minutes. Thirteen source organs that could be identified on PET images were generously delineated on the tomographic slices to ensure that all accumulated radioactivity in each organ was assessed: brain, heart, lungs, spleen, liver, kidneys, gallbladder, red marrow, stomach, testes/ovaries, urinary bladder, and small intestine. Uptake in the source organs was corrected with a recovery coefficient based on the average activity of the frames of the dynamic scan using large ROIs drawn semi-automatically around the body. The concentration of radioactivity, measured without decay correction, was expressed as a percentage of injected dose for each organ. Organ and whole-body radiation exposures were calculated with OLINDA/EXM version 1.1.

PET scanning of monkey brain

One monkey brain scan from the NIH (*Macaca mulatta*, 8.9 kg) and two monkey brain scans from the KI (cynomolgus monkeys, 6.3 and 6.5 kg, respectively) were examined. The NIH experiments were approved by the NIMH Animal Care and Use Committee and performed in accordance with the Guide for Care and Use of Laboratory Animals *(5)*. The KI experiments were approved by the Animal Ethics Committee of the Swedish Animal Welfare Agency and were performed according to the KI "Guidelines for planning, conducting and documenting experimental research" (Dnr 4820/06-600).

At the NIH, the monkey was initially anesthetized with ketamine (10 mg/kg i.m.) followed by 1.6% isoflurane and 98.4% O_2 and placed in prone position in the scanner. Electrocardiogram, body temperature, heart rate, and respiration rate were monitored throughout the scanning session. A microPET Focus 220 scanner (Siemens Medical Solutions; Knoxville, TN) was used to acquire PET images of the brain up to 180 minutes after intravenous injection of ^{18}F-PF-06445974 (218 MBq). PET images were reconstructed using Fourier rebinning+2D filtered back projection with scatter and attenuation correction. To determine the arterial input function, discrete blood samples were drawn manually with increasing intervals from 15 seconds in the beginning of the scan to 30 minutes towards the end.

At the KI, PET scans were conducted using a High-Resolution Research Tomograph (HRRT) (Siemens Molecular Imaging). Anesthesia was induced by intramuscular injection of ketamine hydrochloride (approximately 10 mg/kg) and maintained by administering a mixture of isoflurane (1.5-2.0%), oxygen, and medical air with endotracheal intubation. ECG, heart rate, blood pressure, respiratory rate, oxygen saturation, and temperature were monitored. After ^{18}F-PF-06445974 injection (161 and 159 MBq), the brain was imaged with PET. List-mode data were reconstructed using the ordinary Poisson-3D-ordered subset expectation maximization (OP-3D-OSEM) algorithm, with 10 iterations and 16 subsets including modeling of the point spread function. Blood samples were drawn continuously from the radial artery for the first three minutes using an automatic blood sampling system followed by discrete samples drawn manually for the rest of the scan.

V_T for each region was calculated using a two-tissue compartment model. The time stability of V_T values over time was evaluated by incrementally decreasing the period of brain data from 180 to 90 minutes and by calculating the relative V_T of the truncated scan to V_T of the full scan.

Whole body PET scanning in monkey

Two PET whole-body scans were performed at the NIH on different days in one male rhesus monkey (*Macaca mulatta,* 8.0 kg). A biograph mCT scanner (Siemens Medical Solutions) was used to acquire whole-body PET images for up to 180 minutes after intravenous injection of ^{18}F-PF-06445974 (253 and 200 MBq). The first PET scan was acquired under baseline conditions, that is, without any blocking drugs. In the second PET scan, PF-06445974 (0.1 mg/kg) was intravenously administered 10 minutes prior to the radioligand as the blocking agent. Based on anatomic information from the corresponding CT scan, volumes of interest were delineated on major organs, and time-activity curves were obtained. Uptake for each organ was measured using concentration of radioactivity as standardized uptake value (SUV), which normalizes for injected activity and body mass. Venous blood was used as a

surrogate for arterial blood. For the baseline scan, samples were collected at six timepoints (10, 30, 60, 90, 120, and 180 minutes) to measure the concentration of parent radioligand separated from radiometabolite. The blocking scan with PF-06445974 was terminated after 75 minutes, and the last venous blood was drawn at 60 minutes due to prolonged tachycardia with a maximal heart rate of 190 bpm. For this reason, only 10 to 60 minutes of data from both baseline and blocked scans were used to calculate organ uptake and percentage blockade by PF-06445974. Thus, the average concentration of radioactivity from 10 to 60 minutes ($SUV_{10\text{-}60}$) was divided by the average concentration of parent radioligand during that interval: $SUV_{10\text{-}60}/C_P$.

PET imaging in rats

To determine whether the increasing radioactivity in brain reflected radiometabolite accumulation, two rats (232 g and 193 g) were anesthetized with 1.5% isoflurane and then injected via the penile vein with 42 MBq of ^{18}F-PF-06445974 in 0.9% NaCl solution containing 10% ethanol. Animals were scanned for 180 minutes in a micro-PET Focus 220 camera (Siemens Medical Solutions). One rat was scanned under baseline conditions, and one rat was pre-treated with non-radioactive PF-06445974 (0.1 mg/kg). Blocker was administered intravenously 10 minutes before radioligand injection. Images were reconstructed using Fourier rebinning+2D filtered back-projection with attenuation correction.

Ex vivo studies in rats and mice

Three rats were injected intravenously with ^{18}F-PF-06445974 and sacrificed via thoracotomy at 180 minutes after radioligand injection. Anticoagulated blood was drawn from the myocardium followed by decapitation and brain harvesting. Brain tissues were homogenized in acetonitrile (1.0 mL) and then in water (1 mL). Radio-high performance liquid chromatography (HPLC) was performed on an X-terra® C18 column (10 µm, 7.8 mm×300 mm, Waters Corp, Milford, MA) with a mobile phase of methanol:water: Et_3N (70:30:0.1 by volume) at a flow rate of 3.75 mL/min *(6,7)*.

Brain uptake was also measured in three permeability glycoprotein (P-gp) knockout mice (also called ABCB1 and MDR1 mice) and three breast cancer resistance protein (BCRP) knockout mice (also called ABCG2); P-gp and BCRP are the two most prevalent efflux transporters at the blood-brain barrier *(8)*. HPLC separation was performed on an X-terra® C18 column (10 µm, 7.8×300 mm, Waters Corp.) with isocratic mobile phase of methanol:water: Et_3N: (65:35:0.1 by volume) at flow rate of 5 mL/min.

The in vitro avidity of PF-06445974 as a substrate for human P-gp and BCRP was determined by WuXi AppTec (Cranbury, NJ) in Madin-Darby canine kidney (MDCK) cells transfected with human genes for P-gp or BCRP.

References

1. Zhang L, Chen L, Beck EM, et al. The discovery of a novel phosphodiesterase (PDE) 4B-preferring radioligand for positron emission tomography (PET) imaging. *J Med Chem.* 2017;60:8538-8551.

2. Hammers A, Allom R, Koepp MJ, et al. Three-dimensional maximum probability atlas of the human brain, with particular reference to the temporal lobe. *Hum Brain Mapp.* 2003;19:224-247.

3. Innis RB, Cunningham VJ, Delforge J, al e. Consensus nomenclature for in vivo imaging of reversibly binding radioligands. *J Cereb Blood Flow Metab.* 2007;27:1533-1539.

4. Sprague DR, Fujita M, Ryu YH, Liow JS, Pike VW, Innis RB. Whole-body biodistribution and radiation dosimetry in monkeys and humans of the phosphodiesterase 4 radioligand [(11)C](R)-rolipram: comparison of two-dimensional planar, bisected and quadrisected image analyses. *Nucl Med Biol.* 2008;35:493-500.

5. National Research Council. *Guide for the Care and Use of Laboratory Animals, Eighth Ed.* Washington, DC: National Academies Press; 2011.

6. Terry G, Liow JS, Chernet E, et al. Positron emission tomography imaging using an inverse agonist radioligand to assess cannabinoid CB1 receptors in rodents. *Neuroimage.* 2008;41:690-698.

7. Zoghbi SS, Shetty HU, Ichise M, et al. PET imaging of the dopamine transporter with ^{18}F-FECNT: a polar radiometabolite confounds brain radioligand measurements. *J Nucl Med.* 2006;47:520-527.

8. Löscher W, Potschka H. Blood-brain barrier active efflux transporters: ATP-binding cassette gene family. *NeuroRx.* 2005;2:86-98.

Supplemental Figure S1. Structure of ^{18}F-PF-06445974

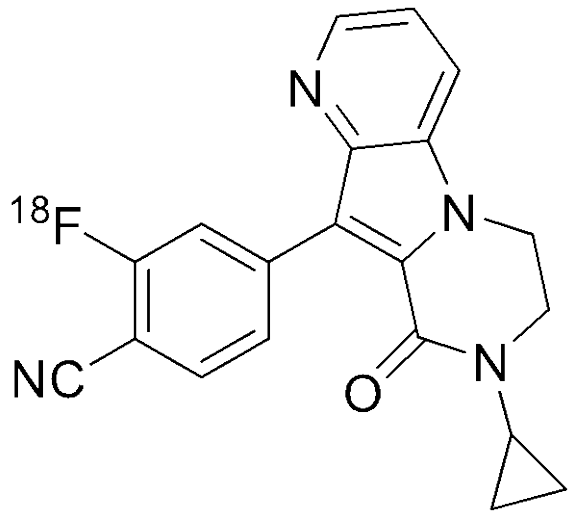

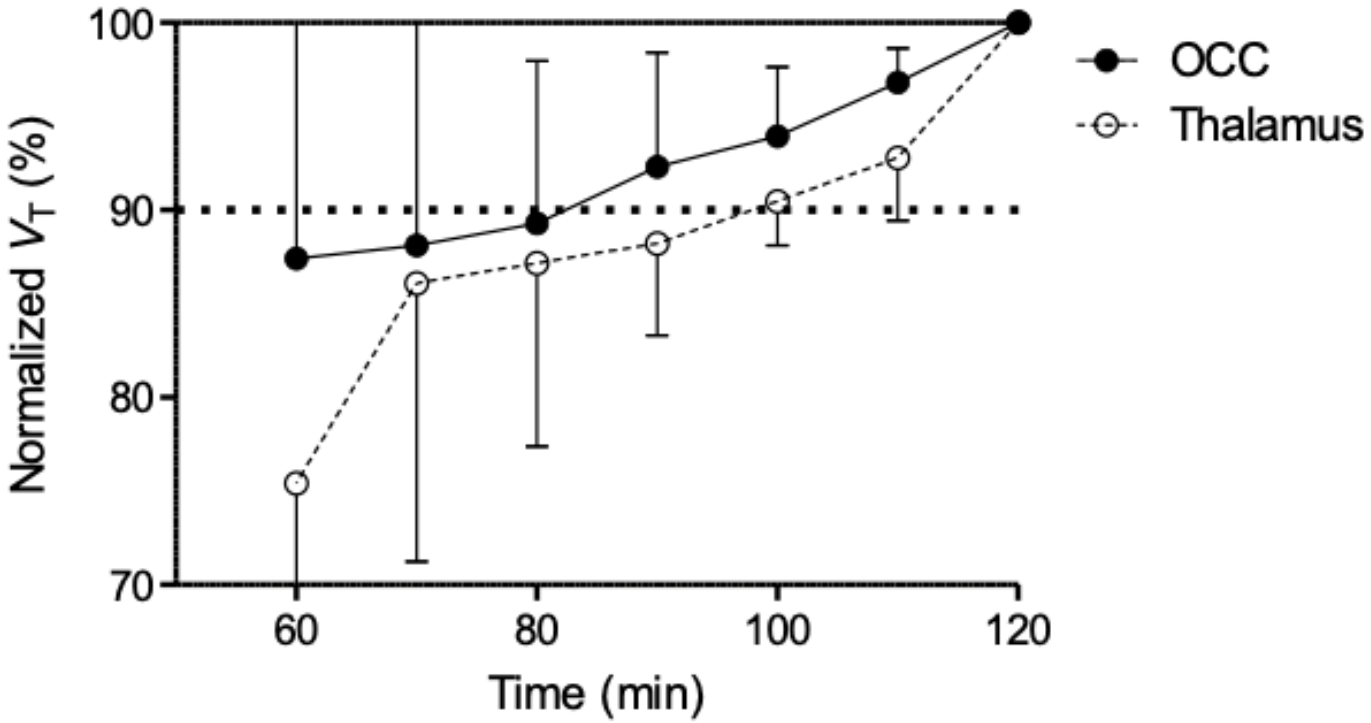

Supplemental Figure S2. Total distribution volume (V_T) values from the five human participants. V_T values never achieved stability during the scans, and a similar linear increase (by 10% during the last 40 minutes) was observed in high- and low-binding regions (thalamus and occipital cortex, respectively).

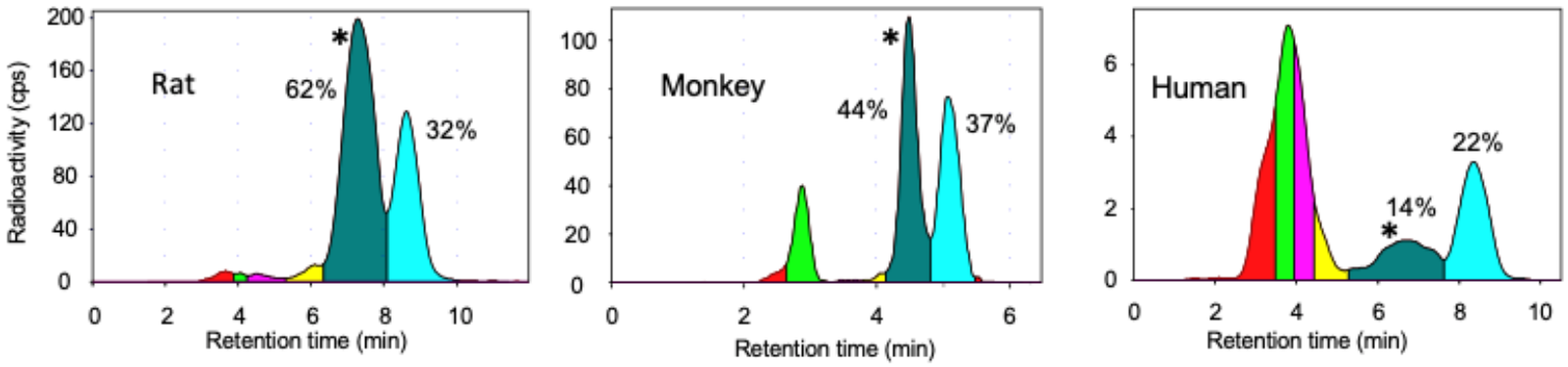

Supplemental Figure S3. Radiochromatogram showing arterial plasma composition after the IV injection of ^{18}F-PF-06445974 into: (A) rat at 180 minutes, (B) monkey at 120 minutes, and (C) human at 120 minutes (C). The green peak enters the brain of transporter knockout mice but is excluded in wild-type mice (Supplemental Fig S3). In the opinion of the authors, this green peak is the problematic radiometabolite that enters human brain. Fortunately, this radiometabolite comprises much less of the plasma radioactivity in humans (14%) compared to rat (62%) and rhesus monkey (44%).

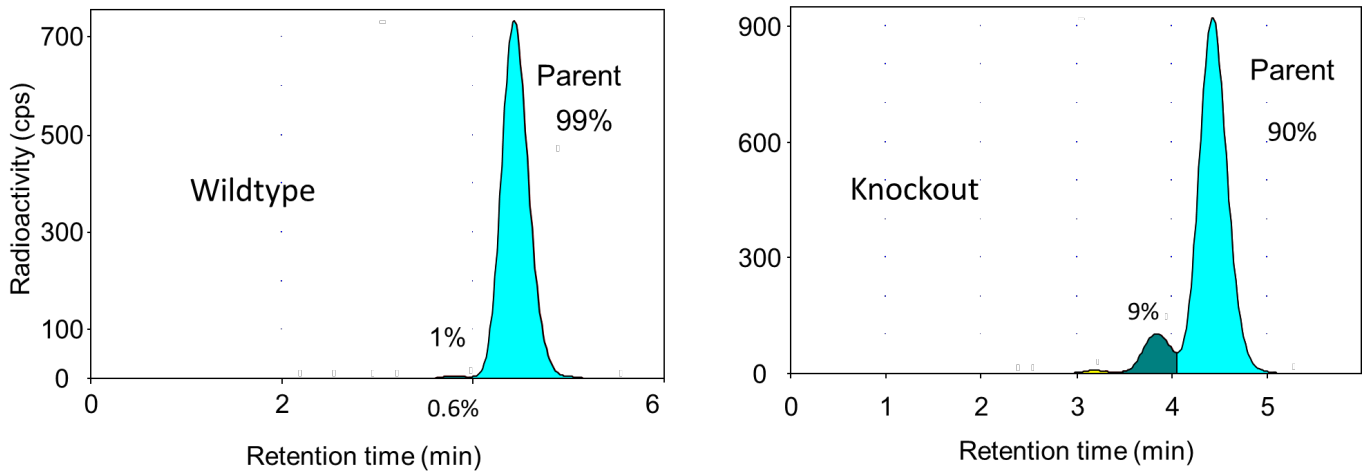

Supplemental Figure S4. Radiochromatogram of radioactivity extracted from the brain of wild-type and efflux transporter knockout mouse. Radioactivity was extracted 120 minutes after IV injection of ^{18}F-PF-06445974. In the wild-type mice, parent radioligand was 99% of all radioactivity, and the adjacent radiometabolite was 1%. In knockout mice, parent radioligand decreased to 90%, while the adjacent radiometabolite increased to 9%.

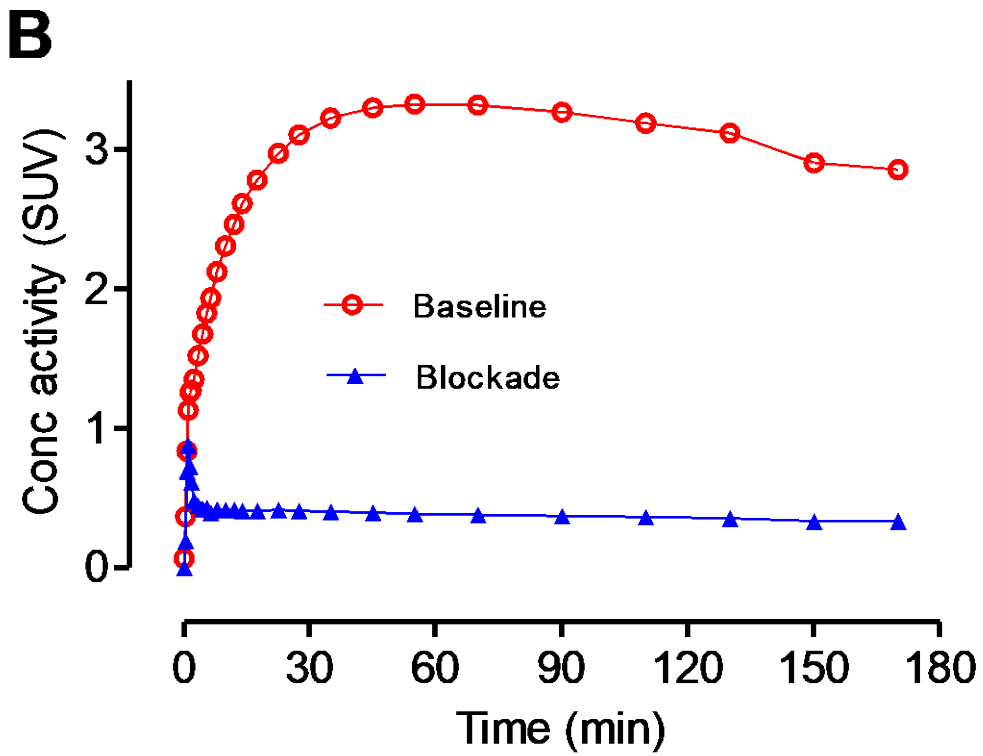

Supplemental Figure S5. The concentration of radioactivity in rat brain at baseline and after blockade by non-radioactive PF-06445974 (1 mg/kg IV injected 10 minutes prior to ^{18}F-PF-06445974). The blocked scan was stable over time, consistent with no radiometabolites accumulating in the brain.

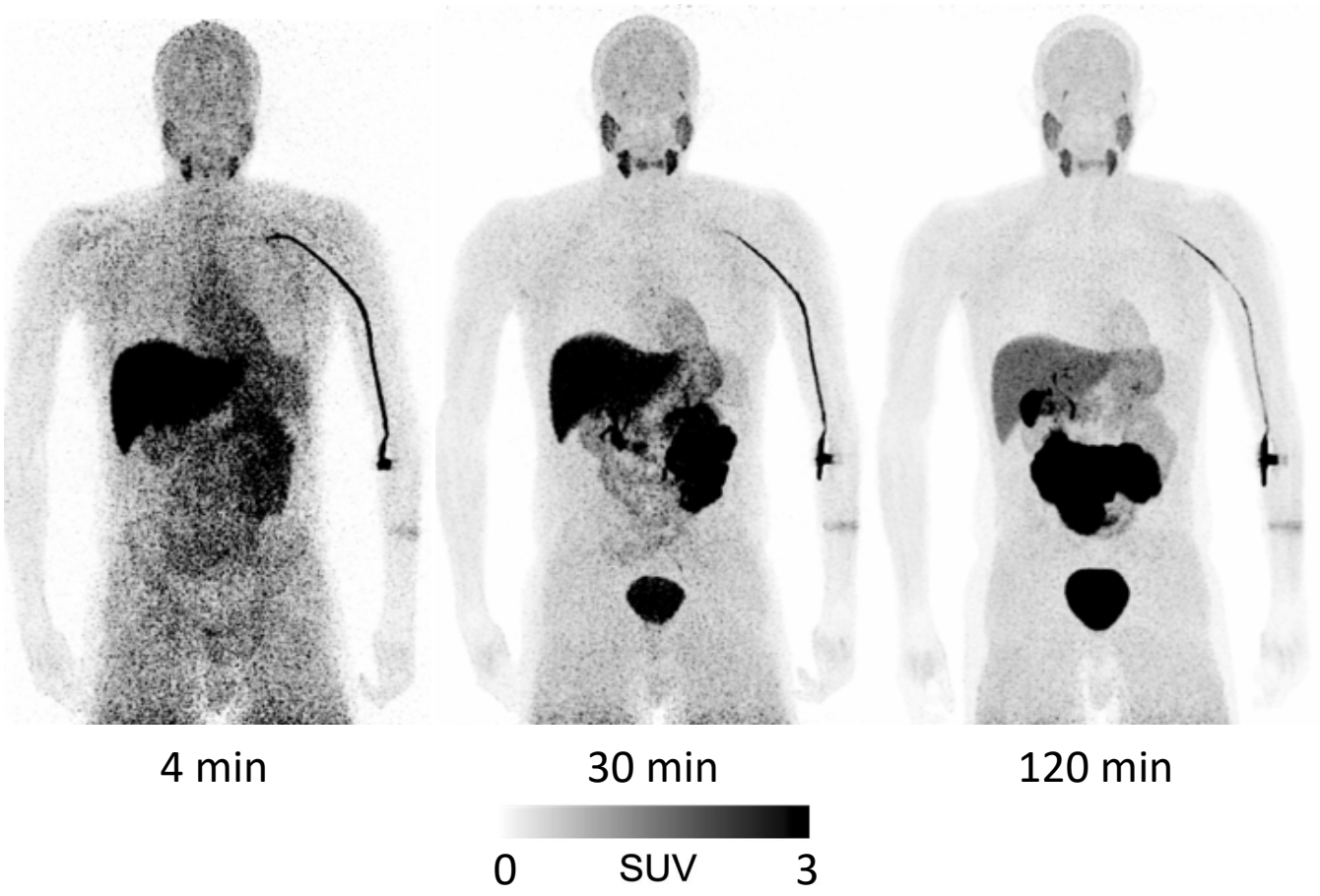

Supplemental Fig S6. Whole-body images of a healthy male human at 4, 30, and 120 minutes after injection of ^{18}F-PF-06445974. The images are displayed in standardized uptake value (SUV) as a two-dimensional compression with maximal intensity projected (MIP) forward. The MIP images emphasize contrast of organs but exaggerate the uptake in small structures like the vein in the left arm. The liver and other excretory organs had the highest concentrations of radioactivity.

Supplemental Table S1. Composition of parent radioligand and radiometabolite in brain and plasma of wild-type and efflux transporter knockout mice.

	% Composition			
	Parent		Radiometabolite	
Tissue	Mean	SD	Mean	SD
Brain				
Wild-type	98.1	1.1	1.8	1.1
Knock-out	90.3	0.6	8.8	0.6
Plasma				
Wild-type	13.3	5.2	68.5	4.2
Knock-out	4.1	0.4	34.6	8.4

Values represent mean ± SD from three mice.

Supplemental Table S2. Avidity of PF-06445974 for two human efflux transporters: BCRP and P-gp

Transporter	Compound	Efflux ratio	Compound + Inhibitor	Efflux ratio
BCRP	Prazosin	9.2	Ko143	0.5
	PF-06445974	5.9	Ko143	0.8
P-gp	Digoxin	38.1	GF120918	2.0
	PF-06445974	2.5	GF120918	0.7

The avidity of PF-06445974 for efflux transport was assessed relative to a known substrate (prazosin for BCRP and digoxin for P-gp) as well as before and after an inhibitor (Ko143 for BCRP and GF120918 for P-gp).
Abbreviations: BCRP: breast cancer resistance protein; P-gp: permeability glycoprotein

Supplemental Table S3. Radiation dose (μSv/MBq) estimates from two healthy volunteers (one male and one female) and one male monkey injected with [^{18}F]PF-06445974

	Radiation dose (μSv/MBq)		
Organ	Male human	Female human	Male monkey
Adrenals	14	19	14
Brain	8	15	10
Breasts	8	12	10
Gallbladder	56	163	21
Lower large intestine	14	17	14
Small intestine	21	17	14
Stomach wall	21	19	13
Upper large intestine	121	28	14
Heart wall	14	16	11
Kidneys	19	28	19
Liver	38	49	19
Lungs	13	22	12
Muscle	11	14	12
Pancreas	25	24	15
Red marrow	11	13	11
Osteogenic cells	15	21	18
Skin	8	10	9
Spleen	18	16	18
Testes/Ovary	15	15	32
Thymus	10	14	12
Thyroid	10	12	12
Urinary bladder	51	59	19
Total body	12	15	12
Effective dose	20	19	17